

Analysis of interface conversion processes of ballistic and diffusive motion in driven superlattices

Thomas Wulf,^{1,*} Christoph Petri,¹ Benno Liebchen,¹ and Peter Schmelcher^{1,†}

¹*Zentrum für Optische Quantentechnologien, Universität Hamburg,
Luruper Chaussee 149, 22761 Hamburg, Germany*

(Dated: November 19, 2018)

We explore the non-equilibrium dynamics of non-interacting classical particles in a one-dimensional driven superlattice which is composed of domains exposed to different time-dependent forces. It is shown how the combination of directed transport and conversion processes from diffusive to ballistic motion causes strong correlations between velocity and phase for particles passing through a superlattice. A detailed understanding of the underlying mechanism allows us to tune the resulting velocity distributions at distinguished points in the superlattice by means of local variations of the applied driving force. As an intriguing application we present a scheme how initially diffusive particles can be transformed into a monoenergetic pulsed particle beam whose parameters such as its energy can be varied.

PACS numbers: 05.45.Ac,05.45.Pq,05.60.Cd

I. INTRODUCTION

Dynamical systems and their transport properties have been studied extensively over the last decades [1], whereas the topic stimulated a vast amount of research when the possibility of directed currents in the absence of a mean force was realised [2–4]. Since the second law of thermodynamics forbids such transport phenomena in equilibrium, these systems have to be constantly driven out of equilibrium. Early works [2–4] were based on noise, i.e. statistical external fields, in combination with spatially asymmetric so called 'ratchet' potentials to overcome the limitations formulated by the second law of thermodynamics and thus to evoke a particle current. These type of systems are of particular interest because they outline a working principal for biological systems such as molecular motors [5, 6] or quantum motors [7]. However, it was soon realised that directed currents can very well be obtained with deterministic external fields, as long as certain spatial- and temporal symmetries in the equations of motion are broken [8], which was investigated afterwards in a vast amount of literature (see [9–15] and references therein). These deterministic ratchets are of particular interest since they might have remarkable applications in nanoscale devices such as electron pumps or transistors [16]. First experimental realisations included semiconductors or semiconductor microstructures where a combination of Laser fields has been applied which led to directed currents in electron ratchets [17, 18]. Directed currents also became a subject of interest in experiments concerning cold atoms in optical lattices [19–22], where additional AC forces are applied to drive the system out of equilibrium and at the same time break the required symmetries that would otherwise pre-

vent transport phenomena. These type of experiments are of particular interest since they allow for a precise control over the system parameters and provide extensive tuneability in the used AC drivings [20, 22].

While the so far mentioned works focus on only time-dependent AC forces, it was found recently that a spatial dependence of these AC forces leads to a diversity of dynamical phenomena [23–25]. The latter studies address the classical dynamics of particles in a lattice with a site-dependent driving. In [23] it is demonstrated how a phase-modulated lattice allows for directed transport even though the driving of each barrier on its own does not break the relevant symmetries [8]. Ref. [24] shows how a ramping of the potential height in combination with a site-dependent driving leads to a patterned deposition of particles. A specific realisation of a site-dependently driven lattice is the one of a block lattice (BL) as introduced in [25], which is reminiscent of semiconductor heterostructures and superlattices. Indeed only recently the possibility of ratchet effects in superlattices of semiconductor heterostructures with a superimposed periodic potential was reported [26, 27]. In the case of [25], the superlattice consists of different blocks containing many individual barriers where the barriers of each block are governed by a certain time-dependence i.e. driving law, whereas different blocks exhibit in general different driving laws. The long time transient dynamics in such a superlattice shows intriguing phenomena like the formation of spatial density oscillations. The latter were explained and analysed by means of conversion processes from diffusive to ballistic (and vice versa) motion at the positions where two neighbouring blocks connect, i.e. at the interfaces of two blocks. However, a rigorous discussion of the processes occurring in a unit cell of such a superlattice -that is a system containing only two blocks each equipped with one of the used driving laws- is still missing and is therefore subject of the present work. In this sense we investigate the diffusive- to ballistic motion conversion processes in detail and explore their influence

* Thomas.Wulf@physnet.uni-hamburg.de

† Peter.Schmelcher@physnet.uni-hamburg.de

on the dynamics of particles leaving the two block system. As a result we obtain peaked velocity distributions for outgoing particles even though their initial conditions are chosen exclusively within the chaotic sea of the underlying phase space. By adjusting parameters in the driving we are able to manipulate these velocity distributions in a controlled manner. Finally, we demonstrate how the insights gained from the two block system enable us to exploit the conversion processes in superlattices build up of many blocks each equipped with a unique driving law. In doing so an initially diffusive particle ensembles is converted into an ensemble with a velocity distribution containing a single peak, whereas both the width as well as the peaks mean velocity can be tuned.

The present work is structured in the following way: In section II we introduce the setup of a block lattice (BL). In section III the dynamics of a single block is discussed. We explore the conversion of diffusive to ballistic motion at distinguished positions in the BL in section IV. Additionally, the influence of these processes for outgoing particles in a simple two block system is discussed in section V. Finally, we investigate the dynamics of superlattices containing several hundred blocks in section VI. Section VII contains our brief conclusions.

II. SETUP AND HAMILTONIAN

The system investigated is a one-dimensional driven lattice consisting of laterally oscillating square potential barriers of equal height V_0 and length l as sketched in Fig. 1. Each barrier is characterised uniquely by its index i .

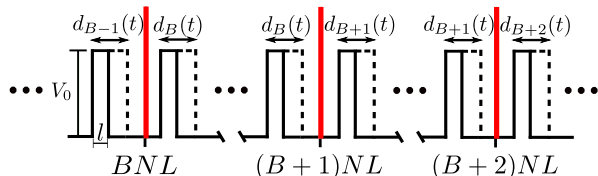


FIG. 1. Sketch of a lattice that consists of differently laterally driven blocks, where the barriers with $NB \leq i < (B+1)N$ are equipped with the same driving law $d_B(t)$.

Furthermore, the barrier positions are time-dependent and described by the so-called 'driving law' $d(t)$, which is chosen such that the i -th barrier remains at all times within an interval of length L expanding from iL to $(i+1)L$. Additionally, the lattice is divided into blocks such that different driving laws $d_B(t)$ (introducing the 'block index' B) are used. In doing so, each $d_B(t)$ governs the barrier motions for the sites $NB \leq i < (B+1)N$ where N denotes the number of barriers within one block and is set to 10^4 throughout this work. The general structure of the driving law is a biharmonic function $d_B(t) = A_B[\cos(\omega_B t) + \sin(2\omega_B t + \Delta\Phi_B)]$ with three parameters A_B , ω_B and $\Delta\Phi_B$ which depend on the block index B . Hence, the resulting classical Hamiltonian for noninteracting particles is given by

$$H(x, p, t) = \frac{p^2}{2m} + \sum_{B=0}^{N_{\text{Bl}}-1} \sum_{i=BN}^{(B+1)N} V_0 \Theta(l/2 - |x - X_{0,i} - d_B(t)|), \quad (1)$$

with N_{Bl} being the number of considered blocks and $X_{0,i}$ the equilibrium position of the i -th barrier (chosen such that the barrier oscillates symmetrically within its unit cell, i.e. $\min|X_{0,i} + d_B(t) - iL| = \min|X_{0,i} + d_B(t) - (i+1)L|$). Additionally, we set the mass $m = 1$ without loss of generality and keep $V_0 = 1.0$, $L = 5.0$ and $l = 1.0$ constant throughout this work.

III. DYNAMICS IN A SINGLE BLOCK

Even though the focus of this work is on composite systems consisting of multiple blocks exposed to different driving laws, these blocks are considered to be large in a sense that the dynamics of a particle within one block can be described by the Poincaré surfaces of section (PSS) as obtained by extending this block to an infinite uniformly driven lattice. It is therefore sensible to discuss the dynamical features such as the transport properties as well as the appearance of the PSS of the uniformly driven lattice. It is well established that the PSS for a uniformly driven lattice can be obtained by exploiting the temporal symmetry of the Hamiltonian: $H(x, t) = H(x, t + T)$. Thus an appropriate choice for the PSS is given by $M = \{(x(t + kT) \bmod L, p(t + kT)) \mid k \in \mathbb{N}\}$ with $T = \frac{2\pi}{\omega}$ being the temporal period. According to this, we record the position taken modulo L and the velocity at certain times $2\pi k$, $k \in \mathbb{N}$ (and call this 'position velocity section'). Such a PSS for $\omega = 1.0$, $A \approx 0.57$ and $\Delta\Phi = 0$ is shown in Fig. 2 b) and features the typical mixed phase space [28], i.e. KAM islands embedded in a chaotic sea which is bounded by the first invariant spanning curve (FISC). Note that the white rectangle is caused by adding the potential energy for particles which are within a barrier at times when position and velocity are recorded. This is done to avoid discontinuities in the PSS caused by the discontinuous potential $V(x, t)$ (cf. [23]). For later usage we show additionally the position velocity section for parameters: $\omega = 1.0$, $A \approx -0.57$ and $\Delta\Phi = 0$ in Fig. 2 a). Note that Fig. 2 a) (b) shows the PSS of the left block (right block) of the corresponding two block system (see section IV).

A second possibility to illustrate the phase space of a uniformly driven lattice is given by the 'phase velocity section' which exploits the spatial symmetry of the Hamiltonian: $H(x, t) = H(x + L, t)$. To this end we record the phases and velocities at certain positions iL . Hence the PSS is obtained from the set of points

$M = \{(t(x + kL) \bmod T, p(x + kL)) \mid k \in \mathbb{N}\}$ and the resulting plot is shown in Fig. 2 d) (again, the PSS for parameters as in Fig. 2 a) is shown additionally in Fig. 2 c) for later usage). Apparently, it features qualitatively the same domains as the position velocity section (Fig 2 b)), i.e. ballistic islands which are embedded in a bounded chaotic sea. However, in contrast to the previous case the chaotic sea appears to be non uniformly filled with trajectories. This seeming contradiction to ergodicity can be resolved easily: According to ergodicity the chaotic sea in Fig. 2 b) can be assumed to be filled with a uniform measure. Hence the number of particles ΔN that pass $x_i = iL$ and therefore contribute to the phase velocity section per time Δt and velocity interval Δv is given by $\frac{\Delta N}{\Delta t} = \rho \frac{\Delta x}{\Delta t} \Delta v = \rho v \Delta v$, where Δx denotes the distance a particle travels in time Δt and ρ is the number of particles per phase space interval. Therefore, the number of particles passing x_i per velocity interval is $\frac{\Delta N}{\Delta v} = \rho v \Delta t$ and hence proportional to v .

We now comment on the transport properties within

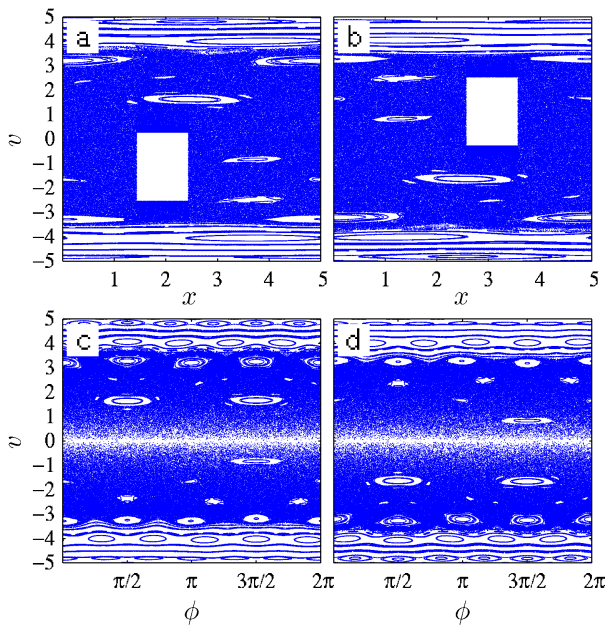


FIG. 2. a) and c) PSS for a uniformly driven lattice with parameters $A \approx 0.57$, $\Delta\Phi = 0$ and $\omega = 1.0$. b) and d) PSS for $A \approx -0.57$, $\Delta\Phi = 0$ and $\omega = 1.0$. a) and b) phases and velocities are recorded at positions $x \bmod L = 0$. c) and d) position x taken modulo L as well as the velocity at times $wt \bmod 2\pi = 0$.

a single block. For $\Delta\Phi_B \neq n\frac{\pi}{2}$ ($n \in \mathbb{Z}$) the biharmonic driving law breaks the time-reversal invariance as well as the parity symmetry of the Hamiltonian and the driven lattice allows for directed transport phenomena [8]. The transport as a function of $\Delta\Phi$ with fixed $A \approx 0.57$ and $\omega = 1.0$ is determined numerically by simulating 10^5 particles in a uniformly driven lattice for 10^6 barrier oscillations and calculating their average velocity after a certain transient time. The results are shown in

Fig. 3 and appear to be in good agreement to the results of a symmetry analysis (cf. [8, 29]) which yields $v_{\text{transport}} \propto -\cos(\Delta\Phi)$. However, there are noticeable deviations, e.g. the reversed sign close to $\Delta\Phi_B = \pi/2$ and $\Delta\Phi_B = 3\pi/2$. Note that these deviations should not surprise us because the authors in [8, 29] considered continuous potentials instead of discontinuous potential barriers. For a more detailed analysis of the dynamics

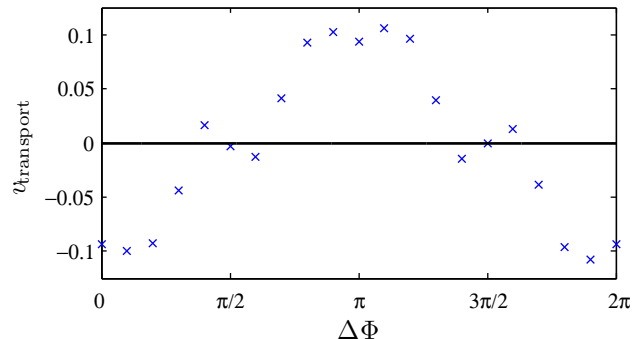


FIG. 3. Numerically determined transport velocity as a function of $\Delta\Phi$ in an infinite uniformly driven lattice with $A \approx 0.57$ and $\omega = 1.0$.

in a uniformly driven lattice, we refer to [23] where this was done in great detail.

IV. INTERFACE CONVERSION IN THE TWO BLOCK SYSTEM

In Ref. [25] it was argued that a BL as introduced in section II offers the opportunity for conversion processes from diffusive- to ballistic motion and vice versa at interface positions where the driving law changes. These type of processes will be analysed in detail throughout this section. We demonstrate in particular their influence on the velocity distribution of a particle ensemble.

A. Interface conversion

Let us introduce the simplest possible finite BL which is build up of only two blocks (i.e. $N_{\text{BL}} = 2$) equipped with different driving laws. Such a system extends from $x_{\text{min}} = 0$ to $x_{\text{max}} = 2NL$ (so the simulation is stopped for a particle once it passes either of these positions) and the driving laws are $d_0(t)$ for $x < x_{\text{mid}} = NL$ and $d_1(t)$ for $x \geq x_{\text{mid}}$. The parameters of $d_1(t)$ are chosen as before ($\omega_1 = 1.0$, $A_1 \approx 0.57$ and $\Delta\Phi_1 = 0$) and thus the dynamics within the 'right block' (RB) can be described by the two PSS in Fig. 2 b) and d). Moreover, Fig. 3 reveals that the used driving law induces a negatively directed current. For the 'left block' (LB) we chose $\omega_0 = 1.0$,

$A_0 \approx -0.57$ and $\Delta\Phi_0 = 0$ yielding $d_0(t) = -d_1(t)$. Hence the corresponding position-velocity section is given by Fig. 2 a) and the phase-velocity section is the one shown in Fig. 2 c). The induced current in the LB is therefore of the same magnitude as in the RB, but positively directed.

To understand how this setup allows for conversion processes it is helpful to consider the dynamics of a particle with initial conditions in the chaotic sea of the LBs phase space. Due to the positively directed current, this particle is in the average transported towards x_{mid} and the chaotic sea for positive velocities in the corresponding phase velocity section (Fig. 2 c)) marks all possible phase space coordinates (v_D, ϕ_D) at which the particle can reach x_{mid} diffusively, while the coordinates belonging to ballistic motion (i.e. within ballistic islands or regular spanning curves above the FISC) (v_B, ϕ_B) are prohibited. However, once the particle passes the interface at x_{mid} its dynamics is no longer governed by the LBs phase space, but by the phase space of the RB, which is appropriately described by the PSS in Fig. 2 d). The crucial observation is that some of the coordinates (v_D, ϕ_D) belonging to diffusive motion in the LB correspond to ballistic motion in the RB. This is best seen by means of a concrete example: Imagine the particle reaches x_{mid} with $(v = 0.8, \phi = 3\pi/2)$, which is inside the chaotic sea of the LBs PSS (Fig. 2 c)). For $x > x_{\text{mid}}$ the particles dynamics is described by the RBs PSS (Fig. 2 d)) where these coordinates correspond to a ballistic island. Hence, this initially diffusive particle would have become ballistic at the interface and we refer to this process as diffusive to ballistic motion conversion. Besides being injected into ballistic islands, the particles can equally well be injected into regular curves above the RBs FISC, because the FISC for positive velocities in the LB is at higher velocities as it is in the RB. To state a general rule, initially diffusive particles can be injected into every regular structure of the RBs PSS which has at least some 'overlap' with the chaotic sea of the LBs PSS. An example of a regular structure in which no injection can occur is the chain of ballistic islands at $v \approx 3.2$ in the RBs PSS (Fig. 2 d)). These islands are 'covered' by a chain of larger islands at the same velocity in the LBs PSS (Fig. 2 c)).

B. Density evolution in the two block setup

After having discussed the process of interface conversion in BLs, we will explore their influence on the time evolution of the particle density in the following.

To this end we propagate the dynamics of a particle ensemble in the two block system, which we introduced in section IV A. As initial conditions we chose uniform distributions for the particles positions as well as their velocities with $0.4NL < x_{\text{ini}} < 0.6NL$ and $-0.1 < v_{\text{ini}} < 0.1$ respectively. Hence the particles are symmetrically distributed around the LBs center and started in the chaotic

sea of the phase space. Naively one might expect that due to the oppositely directed currents in the LB and the RB an accumulation of particles might happen at the interface at x_{mid} . As we shall see in the following, this does not occur due to the previously introduced conversion processes.

Fig. 4 shows snapshots of the normalised particle density at different times. Fig. 4 a) shows the particle density

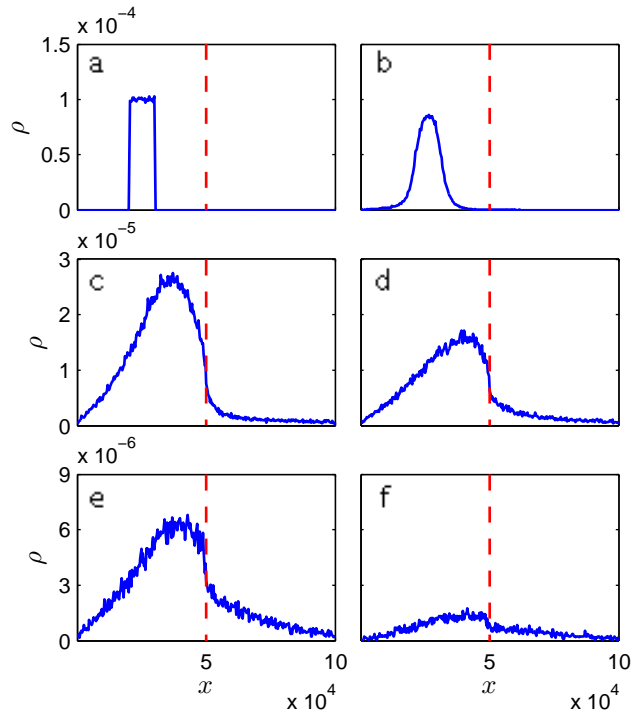


FIG. 4. Particle density at different times in the two block setup ($N_{\text{BI}} = 2$) and $N = 10^4$ yielding $x_{\text{mid}} = 5 \cdot 10^4$ (indicated by the red dashed line) and $x_{\text{max}} = 10^5$. The two driving laws are $d_0(t)$ with $\omega_0 = 1.0$, $A_0 \approx -0.57$ and $\Delta\Phi_0 = 0$ for $x < x_{\text{mid}}$ and $d_1(t) = -d_0(t)$ for $x > x_{\text{mid}}$. All densities are normalised to the initial particle number 10^5 . Snapshots of the particle density are shown for $t = 0$ (a), 10^4 (b), 10^5 (c), $1.8 \cdot 10^5$ (d), $3 \cdot 10^5$ (e) and $5.5 \cdot 10^5$ (f).

$\rho(x)$ for $t = 0$. For $t > 0$ the particle distribution starts to spread and reaches a Gaussian like shape at $t = 10^4$ (Fig. 4 b)). Afterwards the ensemble drifts in positive x -direction and once a sufficient amount of particles arrives at $x_{\text{mid}} = 5 \cdot 10^4$ (marked by the red dashed line in Fig. 4) a sharp decrease of the density emerges at this position (Figs. 4 c) and d)). This effect outlasts until $t \approx 5.5 \cdot 10^5$ (Figs. 4 e) and f)). Finally at $t \approx 10^6$, all particles have left the system at either $x = x_{\text{min}}$ or $x = x_{\text{max}}$ and thus the density in the system is zero.

The broadening of the peak within the LB can be explained by underlying diffusion processes, because all particles are initially restricted to the chaotic sea. In fact, as long as the particles have not reached $x = x_{\text{mid}}$ the ensemble is super-diffusive [23], leading to a fast expansion. On the one hand, the observed average drift of

the ensemble in the LB is explained easily by the positively directed transport in the LB. On the other hand, the fast density decrease is -as mentioned before- somewhat counterintuitive. However, this effect is a straightforward consequence of the in section IV A introduced conversion processes at x_{mid} . According to our discussion, the initially diffusive particles can be injected from the chaotic sea of the LBs PSS into regular structures of the RBs PSS which leads to a fast ballistic motion away from x_{mid} . If the particle remains diffusive, the directed transport brings it back to the interface and an injection from the chaotic sea of the RB to regular structures of the LB is possible. Hence, this process is repeated until an injection occurs and the particle leaves the system at x_{max} (or x_{min}) within a regular structure of the RB (or the LB). The fact that we do not observe a particle accumulation at the interface demonstrates that the conversion process from diffusive to ballistic motion happens on a sufficiently fast timescale to overcompensate accumulation effects caused by the directed currents.

C. Analysis of escaping particles in the two block setup

In the present section we investigate the conversion processes from diffusive to ballistic motions further and illustrate an intriguing hallmark of these processes, namely their influence on the particles phase-velocity distribution.

The starting point is the same two block setup as before and the initial conditions are chosen as before, too. However, instead of discussing the particle positions at certain times as we did in section IV B, we now record the particle velocities and phases at distinguished positions: x_{min} and x_{max} . To this end the phase ϕ and the velocity v for every particle at x_{max} are recorded and the result is shown in Fig. 5 a). In the low velocity regime ($v \lesssim 3.0$) a distinguished island structure is apparent, whereas for higher velocities ($v \gtrsim 3.5$) the particles possess all possible phases from $\phi = 0$ to $\phi = 2\pi$. In between ($3.0 \lesssim v \lesssim 3.5$) the particles appear to have randomly distributed phases and velocities, but do not occupy certain islands.

The islands in the low velocity regime are evidently a consequence of the diffusive to ballistic motion conversion processes. Once a particle which comes from the LB is injected at $x = x_{\text{mid}}$ into a regular structure of the RB, it cannot become diffusive again and travels to $x = x_{\text{max}}$ ballistically. Moreover, it is unlikely for a diffusive particle to reach x_{max} , and indeed impossible if the length of the block tends to infinity, because the local current in the RB is negative. Hence almost every particle in the velocity regime $v \lesssim 3.0$ in Fig. 5 a) is a ballistic one. Note that the island structures can easily be identified with the ballistic islands in the RBs PSS (Fig. 2 d)). In an analogous way we can understand the velocity regime $v \gtrsim 3.5$: These particles are injected into

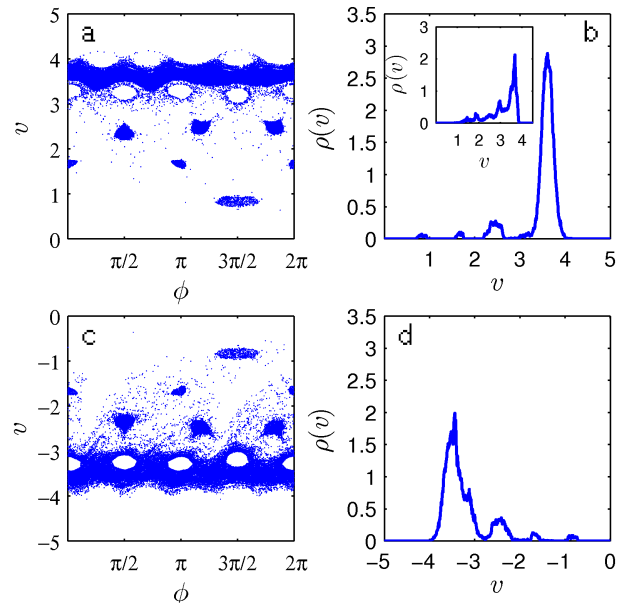


FIG. 5. Properties of the escaping particles for the two block setup with the same parameters as in Fig.4. a) Phases and velocities at $x = x_{\text{max}}$, c) at $x = x_{\text{min}}$. b) and d) show the corresponding normalised velocity distributions $\rho(v)$. The inset in b) shows the velocity distribution for particles which arrive at $x = x_{\text{mid}}$ for their first time.

surface spanning curves above the RBs FISC at x_{mid} . Accordingly, they are not restricted to certain phases. The explanation why certain islands in the velocity regime $3.0 \lesssim v \lesssim 3.5$ are avoided by particles at x_{max} can be given straightforwardly after our previous discussions on the conversion process. As already mentioned in section IV A, these islands correspond to regular structures of the PSS in the RB which have no overlap with the chaotic sea of the LBs phase space and hence no injection occurs.

Finally, we turn our focus on the spreaded particles with $3.0 \lesssim v \lesssim 3.5$: A comparison with the corresponding PSS (Fig 2 d)) reveals that these particles are located within the chaotic sea. Thus they have indeed passed the RB contrariwise to the directed current. To understand why this occurs predominantly in this velocity regime, a short detour on the typical length of Lévy flights in the driven lattice is necessary. To this end we have simulated particles in a uniformly driven lattice with driving law $d_1(t)$ starting at $x = 0$ with $2 \cdot 10^6$ different initial conditions covering the phase space interval ($0 \leq \phi_{\text{ini}} \leq 2\pi$, $-5 \leq v_{\text{ini}} \leq 5$). For every initial condition the number of barriers that the particle passes, before the sign of its velocity changes, is recorded and shown in Fig. 6 (initial conditions leading to regular motion were excluded and are shown in white). Apparently, the number of passed barriers before the velocity is reversed can differ by several orders of magnitude and strongly depends on the initial condition.

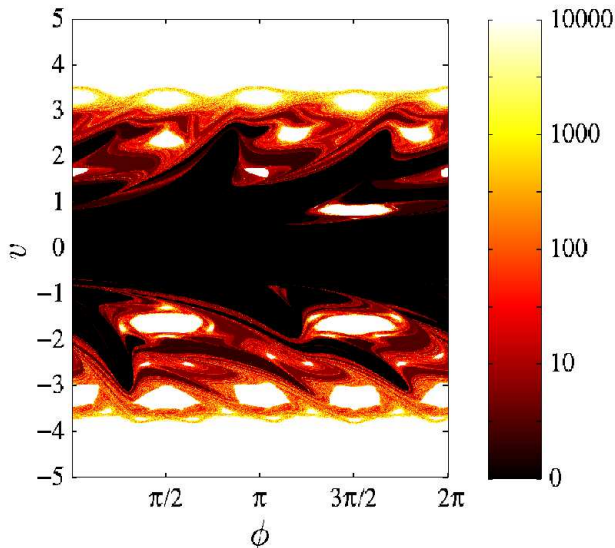


FIG. 6. Length of Lévy flights for particles exhibiting chaotic dynamics in a uniformly driven lattice with driving law $d_1(t)$ (parameters as in Fig. 2 d)). The white regions correspond to initial conditions leading to regular motion.

Most interesting for our purpose is the observation that particles started in the velocity regime $3.0 \lesssim v \lesssim 3.5$ exhibit extraordinary long 'ballistic like' flights, which can be at the order of a few thousand barriers. Hence it is more likely for a particle -that remains diffusive once it passes x_{mid} - to reach x_{max} before being transported back to x_{mid} if it is within this region of extraordinary long Lévy flights. Indeed, a comparison of Fig. 6 with Fig. 5 a) reveals, that the regions of long Lévy flights coincide with the ones where diffusive particles reach x_{max} .

Even though the overall appearance of the plot shown in Fig. 6 does strongly depend on the used parameters in the driving law, it is -for later usage- worth emphasising that the tendency for fast particles to exhibit much longer Lévy flights than slower ones is a rather general feature in the driven lattice. This is mainly caused by two facts: Firstly, the lattice becomes a smaller perturbation for faster particles. Hence the average velocity change at a collision with a barrier is small for a particle which is close to the FISC (note that it is indeed zero for particles on the FISC) and as a consequence it takes many collisions with the barrier before a notable impact on the particle velocity occurs. Secondly, for particles with large initial velocities it is likely to become sticky to the FISC which -according to the discussions in [23]- leads to long ballistic flights.

Besides leaving the system at x_{max} , there is also the possibility for a particle to leave the system at x_{min} . Again, phase and velocity at this particular position are recorded and shown in Fig. 5 c). This plot features qualitatively the same occupied domains as the one for x_{max} but now mirrored at $v = 0$: Distinguished island

structures belonging to a regular ballistic dynamics for less negative velocities, particles obeying chaotic dynamics which avoid ballistic islands for $-3.5 \lesssim v \lesssim -3.0$ and particles on regular spanning curves with velocities $v \lesssim -3.5$. The main difference appears to be the larger amount of spreaded diffusive particles for velocities with $v \gtrsim -3$ which do not correspond to ballistic islands.

Both the difference as well as the similarity to the x_{max} plot can be understood intuitively: Since the ensemble is initially located around the center of the LB, the number of barriers that these particles have to pass diffusively and opposite to the direction of the local current is roughly 5000, while it would be 10000 for particles that have reached x_{mid} . Consequently, most of the spread diffusive particles seen in Fig. 5 c) are particles which have never reached x_{mid} . In contrast to this, the particles reaching x_{min} within either ballistic islands or regular spanning curves have obviously passed x_{mid} at least twice, because otherwise they could not be injected into the corresponding regular structures of the LB. Note that once a particle reaches x_{mid} , it is injected into the PSS of the RB with $d_1(t)$ for positive velocities and into the PSS of the LB with $d_0(t)$ for negative velocities. Since we chose $d_0(t) = -d_1(t)$, the ballistic islands apparent in Fig. 5 c) are the same as in Fig. 5 a), but mirrored at $v = 0$.

D. Injection probabilities into different regular structures

So far we have seen that the two block system allows for diffusive to ballistic motion conversion processes. In this section we further investigate this phenomenon and discuss how likely injections into different regular regimes such as ballistic islands or spanning curves above the FISC are.

To get some insight it is instructive to compare the normalised phase integrated velocity distributions at x_{max} (Fig. 5 b)) with the one at x_{min} (Fig. 5 d)). The for our purpose crucial observation is that the peak at high velocities ($|v| \gtrsim 3$) is less pronounced at x_{min} , and that the peaks corresponding to the ballistic islands appear slightly stronger populated (hardly visible) compared to the peaks in the distribution at x_{max} . This effect can partially be explained by the larger number of diffusive particles at x_{min} , leading to a broadening of the high velocity peak, but is also caused by certain characteristics of the injection process at x_{mid} as we shall explain in the following.

A further understanding can be obtained by considering the velocity distributions for outgoing particles for a given number of times a particle has crossed x_{mid} before it leaves the system (in the following we refer to this number as n_{cr}) as shown in Fig. 7. Apparently, for $n_{\text{cr}} = 1$ (Fig. 7 a)) the distribution features a very pronounced peak at velocities between 3 and 4, which

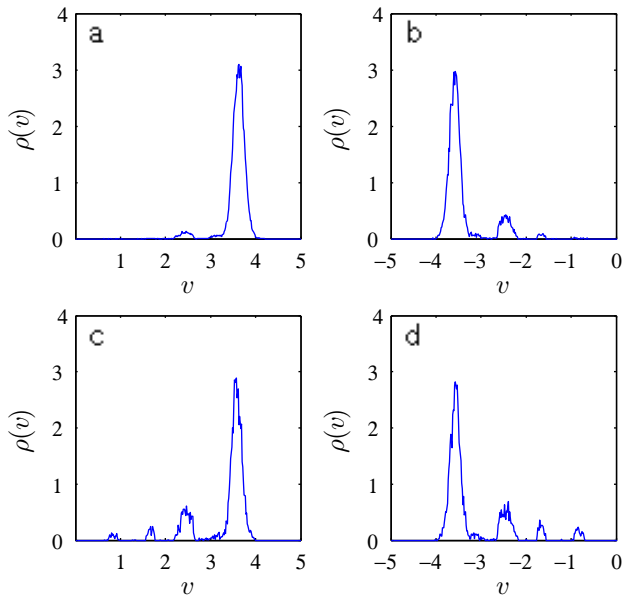


FIG. 7. Normalised and phase integrated velocity distributions at x_{\max} in a) and c) and at x_{\min} in b) and d) for the subset of the ensemble which has crossed x_{mid} n_{cr} times (a) $n_{\text{cr}} = 1$, b) $n_{\text{cr}} = 2$, c) $n_{\text{cr}} = 3$ and d) $n_{\text{cr}} = 4$). Parameters as in Fig. 4.

appears stronger populated compared to the peak in the total velocity distribution at x_{\max} shown in Fig. 5 b). On the contrary, the peaks corresponding to ballistic islands at smaller velocities are clearly weaker pronounced. In the $n_{\text{cr}} = 2$ case it is less apparent, but the islands at small velocities are still less pronounced as for the total distribution in Fig. 5 d). For $n_{\text{cr}} = 3$ this effect is reversed and the low velocity peaks contain relatively more particles than they do in the total velocity distribution. Finally, particles leaving the system with $n_{\text{cr}} = 4$ are very similar to the ones with $n_{\text{cr}} = 3$ and no obvious deviation in the velocity distributions is observed. It will become clear later, that this behaviour is strongly correlated with a different effect which is worth mentioning at this point: Not only the normalised distributions differ for different n_{cr} , but the probabilities for a particle to leave the system after a certain number of crossing n_{cr} are different as well. Hence, the injection probabilities into any kind of regular structures $p_{n_{\text{cr}}}$ has to be different for different n_{cr} and we indeed found numerically, that the probability for a particle to be injected into a regular structure while it passes x_{mid} for the first time is $p_1 \approx 0.49$, while it is $p_2 \approx 0.24$ for the second passing of x_{mid} and approximately $p_i \approx 0.15$ for $n_{\text{cr}} > 2$.

To understand both the different overall injection probabilities $p_{n_{\text{cr}}}$ for different n_{cr} as well as the different appearances of the corresponding velocity distributions, an argument which combines the length of Lévy flights in different regions of the phase space (as discussed before

and shown in Fig. 6 for the RB and to be mirrored at $v = 0$ for the LB) together with the ergodicity property is required: Due to ergodicity parts of the phase space corresponding to long ballistic flights must be visited less frequently, but once a particle gets there, it stays for a comparably long time. Hence, a particle initially started very close to x_{mid} with a small velocity, reaches the interface after only a few collisions and as a consequence it is unlikely to reach the high velocity regime for such a particle. On the contrary, for a particle that started far -say some thousand barriers- away from x_{mid} , it is likely that the particle reaches this high velocity domain at some point. Once it possesses such a high velocity, the length of its Lévy flight is of the same order as its distance from x_{mid} and the particle typically reaches the interface while being still confined to this domain of phase space. We remark that this effect can easily be observed in the velocity distribution at x_{mid} for particles which reach this position for their first time as shown in the inset of Fig. 5 b). Apparently the distribution reveals a strongly pronounced peak at velocities close the LBs FISC in agreement with the previous discussion. Since these fast particles in the LB have velocities $v \gtrsim 3.5$ they are injected into regular spanning curves above the FISC of the RB, which explains why particles at the first injection process have extraordinary high velocities and consequently why p_1 is extraordinary large. Additionally, it illustrates why this domain appears to be strongly populated for $n_{\text{cr}} = 1$ (cf. Fig. 7 a)).

Following the same arguments, the velocity distribution for $n_{\text{cr}} = 2$ as well as the slightly enhanced value of p_2 compared to p_i with $i > 2$ can be understood too. Because the particles are extraordinary fast at their first arrival at x_{mid} , a comparably large fraction of particles which remain diffusive is injected into the part of the RBs PSS corresponding to long Lévy flights (cf. Fig. 6). Hence they surpass a large number of barriers in the RB which is at the order of 10^3 before their velocity is reversed for the first time. Afterwards, they are most likely transported towards x_{mid} due to the negatively directed current in the RB. Now the same argument as before holds: because these particles are relatively far away from x_{mid} , they reach x_{mid} predominantly with a high velocity. Hence, this domain is still strongly populated for the $n_{\text{cr}} = 2$ injection process and p_2 is slightly enhanced. By now most of the fast particle have left the system and the still diffusive ones are transported back to x_{mid} after only a few collisions. Consequently, the injection probability into the high velocity domain is suppressed for larger n_{cr} .

V. CONTROLLING THE VELOCITY DISTRIBUTION

We have seen in section IV that a BL consisting of differently driven blocks allows for the conversion of diffusive- to ballistic motion and vice versa at interfaces where the driving law changes. As a hallmark of these processes, we obtained velocity distributions with pronounced peaks at the velocities associated to regular structures in the underlying phase space. In the following section we investigate to what extent these conversion processes can be exploited to modulate the velocity distribution for outgoing particles in a controlled manner by adjusting parameters in the driving law.

Again we focus on the two block setup ($N_{\text{Bl}} = 2$, $N = 10^4$) with two different driving laws $d_0(t)$ for $x < x_{\text{mid}}$ and $d_1(t)$ for $x \geq x_{\text{mid}}$. The parameters in $d_0(t)$ remain as before throughout the entire section and thus a positively directed current is induced in the LB. On the contrary, each parameter in $d_1(t)$ is varied separately and its influence on the phase velocity distributions at x_{max} and x_{min} shall be studied. To this end we simulate an ensemble of 10^5 particles (initial conditions as in section IV) until all particles left the two block system.

However, before we begin a detailed analysis of the phase velocity distributions for outgoing particles at x_{max} in various parameter regimes it is sensible to have a brief discussion on their expected parameter dependence: Assuming a negatively directed current in the RB (which will be the case in most of the studied scenarios), we can expect that the particles arrive at x_{max} predominantly within either ballistic islands or regular curves above the FISC corresponding to the RBs phase space. Hence the phase velocity distributions at x_{max} provide an 'image' of all the regular structures in the PSS of the RB which have overlap with the chaotic sea of the LBs PSS (Fig. 2 c)). Additionally to the ballistic particles some diffusive particles are expected to reach x_{max} if the underlying phase space of the RB possesses regions of long Lévy flights. Provided with these arguments we are able to explain most of the phenomena occurring in the following sections.

A. Frequency variations

To begin with, we explore how a change of ω_1 manifests itself in the particles' velocity distributions when they leave the system at either x_{max} or x_{min} . The other parameters of $d_1(t)$ are kept constant at $A_1 \approx 0.57$ and $\Delta\Phi_1 = 0$ (inducing negatively directed currents in the RB for all values of ω_1).

Figs. 8 a)-d) show the phase velocity distribution at x_{max} with varying frequencies $\omega_1 = 0.05, 1.50, 1.65$ and 4.00 . Fig. 8 a) corresponds to the low frequency ($\omega_1 = 0.05$) regime where the barriers within the RB move very slowly compared to the barriers inside the LB. It shows a broad velocity band which is sharply confined

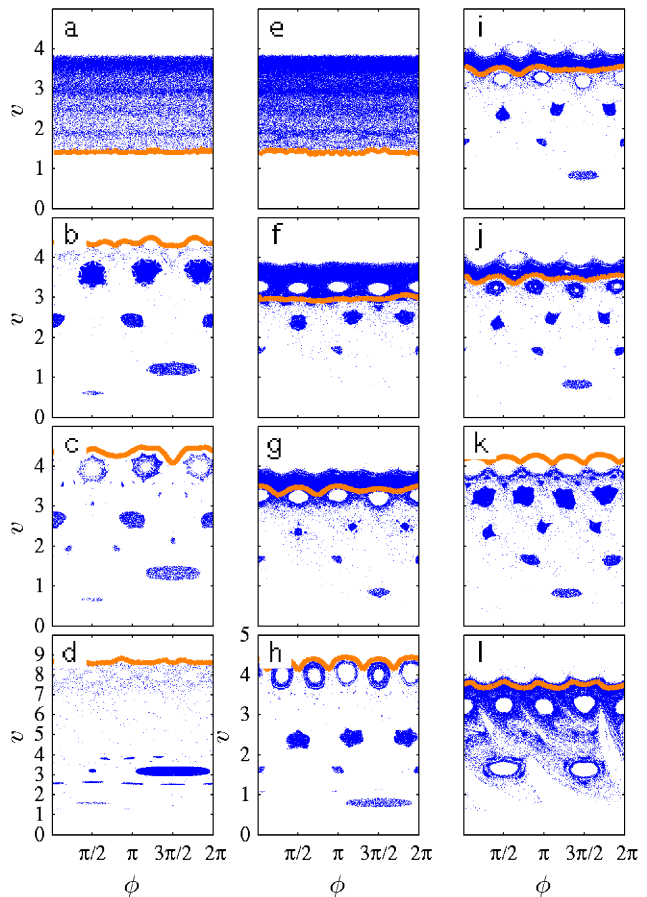


FIG. 8. Phase velocity distributions at $x = x_{\text{max}}$ for a two block system with $d_0(t)$ as in Fig. 4. The orange line indicates the FISC in the PSS of the RB. For $d_1(t)$ the parameters are $A_1 \approx 0.57$, $\Delta\Phi_1 = 0$ and $\omega_1 = 0.05, 1.50, 1.65, 4.00$ for a)-d). For e)-h) we have $\Delta\Phi_1 = 0$, $\omega_1 = 1.0$, and $A_1 = 0.02, 0.40, 0.50, 1.00$. For i)-l) we have $A_1 \approx 0.57$, $\omega_1 = 1.0$, and $\Delta\Phi_1 = 0.1\pi, 0.2\pi, 0.5\pi, 1.0\pi$.

between $v \approx 1.4$ and $v \approx 3.8$ where particles reach x_{max} without any apparent restrictions on their phases. This can be explained straightforwardly, by considering the expansion of the chaotic sea. As argued in [23], the velocity for particles on the first invariant spanning curve (FISC) limits the chaotic sea and can be estimated by $v_{\pm} = \pm \dot{d}_{\text{max}}^{\pm} \pm \sqrt{2V_0}$ where \pm correspond to positive or negative velocities and $\dot{d}_{\text{max}}^{\pm}$ is the maximal barrier velocity in either positive- or negative direction. For a small frequency ω_1 the maximal velocity of the barrier in any given direction becomes small as well, leading to a FISC in the RB at very low velocities (for illustration we show the FISC in the RBs PSS as an orange line in Fig.8). According to our previous discussion, almost all particles are injected into regular spanning curves above the RBs FISC at x_{mid} and are able to reach x_{max} at arbitrary phases. The sharp cutoff at $v \approx 1.4$ can be explained by employing the approximation of a static potential which yields a minimal particle velocity of $v = \sqrt{2V_0} \approx 1.41$ to

surpass the barrier.

Increasing ω_1 in the RB leads us to a second regime, where the FISCs in both blocks are at similar velocities and we show the corresponding phase velocity distribution for $\omega_1 = 1.50$ in Fig. 8 b). The distribution reveals the expected domains of particles in ballistic islands and some diffusive particles close to the FISC in the RBs phase space. Both features are straightforward consequences of the previous discussions and we refrain from a reiteration of the arguments. However it is appealing to explore how the overall picture changes for a small variation in ω_1 . To this end the phase velocity plot for another frequency of $\omega_1 = 1.65$ is presented in Fig. 8 c). Apparently, the phase velocity distribution of particles at x_{\max} looks similar to the one for $\omega_1 = 1.50$. Nevertheless there are some differences worth emphasising. First of all, the 'large' islands survive the frequency change, but are shifted to slightly higher velocities for an increased ω_1 . Additionally, the islands at $v \approx 4.0$ appear now emptied around their center. By comparing the PSS of the

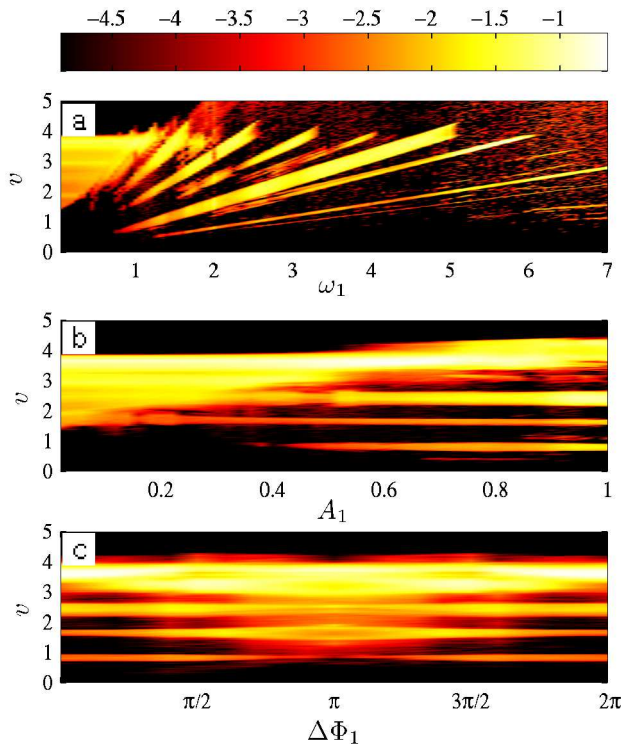


FIG. 9. Phase-integrated velocity distributions at x_{\max} (setup as as in Fig. 4) on a logarithmic scale for variations of a) ω_1 , b) A_1 and c) $\Delta\Phi_1$. Remaining parameters as in Fig. 8.

LB and the RB we see that those depleted parts of the ballistic islands in the RBs phase space are at velocities which are partially above the FISC of the LB. Since the injection at x_{mid} can only occur for regular curves within the island that are at least in parts covered by the chaotic sea of the LBs phase space and the outer curves in each island reach to lower velocities than the inner curves, the latter ones are depopulated first.

Finally, we address the regime where the FISC in the RB is at much higher velocities than the FISC in the LB, which is realised for $\omega_1 \gg \omega_0$ and the phase velocity distribution is shown exemplarily for $\omega = 4.0$ in Fig 8 d). Apparently, only the island initially at ($\phi \approx 3\pi/2$, $v \approx 1.2$) survives, but is shifted to considerably higher velocities ($v \approx 3.0$). Moreover, we notice a comparably large portion of diffusive particles at high velocities ($7.0 \lesssim v \lesssim 9.0$) below the FISC in the RB. To visualise the results over a broad range of ω_1 , we integrate the phase velocity distributions over the phase and normalise each in the range $\omega_1 = 0.05 - 7.00$ (see Fig.9 a)). Evidently, the particles arrive within a

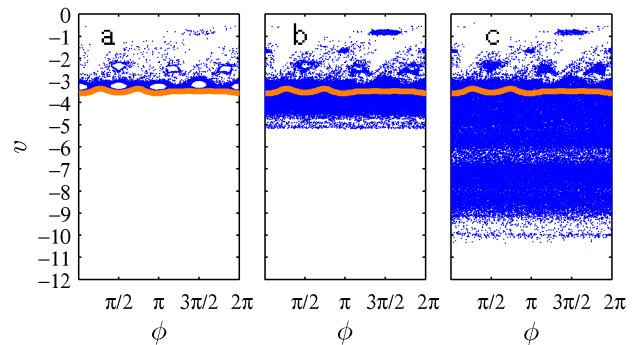


FIG. 10. Phase velocity distributions for particles which exit at x_{\min} for a) $\omega_1 = 0.05$, b) $\omega_1 = 1.50$ and c) $\omega_1 = 4.00$ (remaining parameters as in Fig.4). The orange line indicates the FISC position in the LB.

broad range of velocities for small ω_1 's, while they are restricted to certain comparatively narrow velocity intervals at higher frequencies. Both can be understood within the above analysis: For small frequencies the particles are predominantly injected into regular spanning curves and for higher ones mainly into individual ballistic islands. These islands are shifted to higher velocities for increasing ω_1 and once they pass the FISC of the LB they simply disappear. What these velocity distributions reveal additionally is that the islands mean velocities tend to increase linearly with ω_1 . This is caused by the fact, that ballistic islands correspond to trajectories synchronised with the barrier oscillations in a way that every collision with the barrier occurs at distinguished phases. Each island is thereby characterised by its winding number n which is defined (within a block) as the number of unit cells the particle passes within one period T . Hence the average velocity of a particle trapped in such an island is given by $v_n = \frac{Ln}{T} = \frac{Ln}{2\pi} \cdot \omega_1$ and thus proportional to ω_1 .

Besides the possibility for leaving the system at x_{\max} particles can also exit at x_{\min} . Although, the parameters in the LB are kept constant, the parameters in $d_1(t)$ can have a substantial influence on the particle dynamics at x_{\min} due to conversion processes after multiple crossing of x_{mid} . This is demonstrated in Fig. 10 where the phase velocity distributions are shown exemplarily for

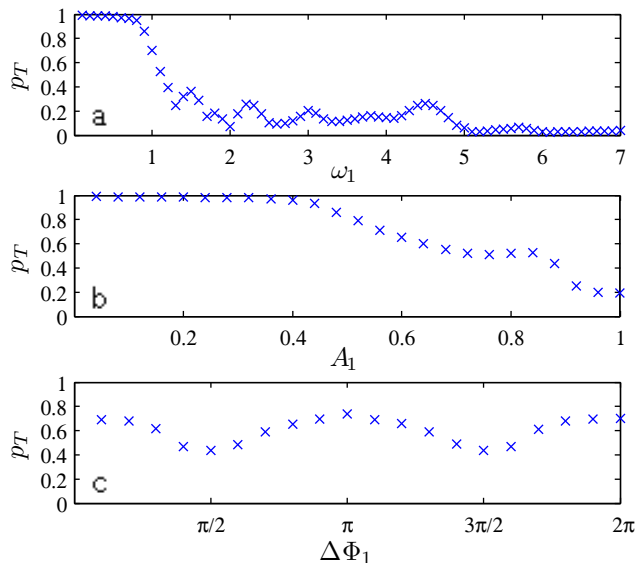


FIG. 11. Transmission probability p_T as a function of a) ω_1 , b) A_1 and c) $\Delta\Phi_1$. Remaining parameters as in Fig. 8.

$\omega_1 = 0.05, 1.50$ and 4.00 . Again let us discuss first the small frequency regime (Fig. 10 a)). Since the FISC in the RB is at very low velocities for $\omega_1 = 0.05$, all the fast particles are immediately injected into regular curves and therefore leave the system at $x = x_{\max}$. Consequently, there is little probability for a particle to be re-injected into regular structures in the LB once it has entered the RB and as a consequence all the particles seen in Fig. 10 a) are diffusive ones. More precisely, these are mainly particles that never reached x_{mid} , i.e. the 'diffusive background' which is always present at x_{min} , independent of the parameters of $d_1(t)$ and consists of approximately 20% of all particles (note that this number tends to zero if the size of a block tends to infinity).

For increasing ω_1 the situation changes substantially, as demonstrated for $\omega_1 = 1.50$ in Fig. 10 b). Evidently, some of the ballistic islands at minor negative velocities are filled. Additionally, we observe particles on regular spanning curves below the FISC, which were not present in the case $\omega_1 = 0.05$. However, before we give an explanation by means of the underlying PSS we remark that the relevant parts of the phase space are now the ones for negative velocities (cf. Figs. 2 c) and d) for $v < 0$). By keeping this in mind, the difference of Fig. 10 b) compared to Fig. 10 a) can be understood intuitively by the FISC position: Since the FISC for negative velocities in the RB is now lower than the one for negative velocities in the LB, there is significant overlap of the chaotic sea in the RB and ballistic islands- as well as invariant curves below the FISC in the LB. Consequently, these parts of phase space in the LB can be populated by diffusive particles in the chaotic sea of the RB which are transported back to x_{mid} by the negatively directed current. The same arguments hold for the high frequency domain

that is exemplarily shown for $\omega_1 = 4.00$ in Fig. 10 c). Since the FISC for negative velocities in the RB is at lower, i.e. more negative, velocities compared to the case $\omega_1 = 1.50$ the particles which penetrate into the RB diffusively can now be injected into regular curves of the LB at more negative velocities and therefore reach x_{mid} faster than before. Note that even though the particles have no apparent modulation in phase, they are not uniformly distributed within the accessible range of velocities, which can be traced back to the underlying PSSs. For example the local minimum at $v \approx -6.5$ (cf. Fig. 10 c)) is caused by a chain of ballistic islands embedded in the RBs chaotic sea which is decreasing the overlap and therefore the injection probability into regular structures of the LB within this velocity regime.

We conclude this chapter with some remarks on the impact of a varying frequency in the RB on the transmission probability p_T through the interface. i.e. the ratio of the particles reaching x_{\max} and the total number of particles reaching x_{mid} . Its dependence on ω_1 is shown in Fig. 11 a) (note that we omit the diffusive background, i.e. we only take particles into account that have actually reached x_{mid} at least once). For small frequencies almost all particles are transmitted, while this changes drastically for $\omega_1 \gtrsim 1.0$ when p_T starts to oscillate around $p_T \approx 0.2$ until it is again decreased above $\omega_1 \approx 4.5$ to $p_T \approx 0.05$ where it appears to saturate. All three regimes can be understood by means of our previous discussions: Since the particles arriving at x_{mid} for their first time have predominantly high velocities ($3.5 \lesssim v \lesssim 4.0$) (cf. the inset of Fig. 5 c)), p_1 (and hence p_T) is large whenever regular structures in the phase space of the RB are located within this velocity regime. For small ω_1 this is the case because the PSS in the RB is in this velocity regime filled with regular curves above the corresponding FISC. For $\omega_1 > 1$ this is no longer true (cf. for example 8 b)) and thus the particles rely on injection processes into ballistic islands rather than regular spanning curves to surpass the RB ballistically. Consequently p_T drops significantly. For larger frequencies p_1 (and therefore p_T) increases whenever one of the ballistic islands in the RBs phase space is in the velocity regime $3.5 \lesssim v \lesssim 4.0$ (cf. Fig. 9 a)) and decreases once this island disappears because it is above the FISC of the LB, which explains the oscillatory behaviour of p_T for $1.0 < \omega_1 < 4.5$. At $\omega_1 \approx 4.5$ the last ballistic island corresponding to an integer value of the winding number n disappears and thus p_T drops further.

B. Amplitude variations

Analogous to the previous discussion, we explore how a change of the oscillation amplitude A_1 in the RB affects the particle properties for fixed values of $\omega_1 = 1.0$ and $\Delta\Phi_1 = 0$. As before the parameters in $d_0(t)$ remain unaltered. The corresponding phase velocity distributions at x_{\max} are shown exemplarily in Figs. 8 e)-h). The

regime of small amplitudes is represented by Fig. 8 e) which shows the particles phase velocity plot at x_{\max} for $A_1 = 0.02$. Apparently, the particles are restricted to the same velocity interval as for the 'small frequency regime' illustrated in 8 a), namely $1.4 \lesssim v \lesssim 3.8$. The interpretation in terms of a quasi static barrier motion as provided previously for the case of small frequencies holds also here for the case of a small amplitude motion. Accordingly, most particles are injected into regular spanning curves above the FISC of the RB once they pass x_{mid} for the first time. If we increase A_1 the FISC is shifted to higher velocities and reaches $v \approx 3.0$ for $A_1 = 0.40$. The associated phase velocity plot is shown in Fig. 8 f). For velocities below the FISC we observe the familiar island like structure. Particles can still be injected into curves above the FISC, where a chain of islands is avoided ($v \approx 3.2$). The latter one is caused by the fact, that these ballistic islands in the phase space of the RB have no overlap with the chaotic sea in the LB. This is due a chain of larger ballistic islands in the LBs phase space (Fig. 2 c)) at the same velocity.

Fig. 8 g) shows the corresponding graph for a slightly increased amplitude $A_1 = 0.50$ and reveals that the FISC is -as expected- shifted to higher velocities. Furthermore, a region containing a considerable number of diffusive particles evolves at $3.0 \lesssim v \lesssim 3.5$ followed by an island structure for even lower velocities. The surprisingly high number of diffusive particles at velocities slightly below the FISC is caused by extraordinary long Lévy flights within this region due to a chain of cantori at $v \approx 3$. As a consequence of the small flux through this chain, the dwell time for particles in this part of the phase space is enhanced drastically [23]. According to our previous discussions in section IV C this enhances the probability for diffusive particles to reach x_{\max} in this part of the phase space.

Fig. 8 h) shows the phase velocity distribution at x_{\max} for a large amplitude $A_1 = 1.0$. Evidently, the FISC in the RB is in this case at higher velocities than it is in the LB. Thus, mainly particles within ballistic islands reach x_{\max} . As we observed for a high frequency (cf. Fig. 8 c)), some of the islands are partially above the LBs FISC and their inner curves are therefore depleted. The phase integrated results over a range of amplitudes $A_1 = 0.02 - 1.0$ is shown in Fig. 9 b). Similar to what we observe for the frequency dependence the particles cover a broad velocity interval ($1.5 \lesssim v \lesssim 4.0$) for small amplitudes. With increasing A_1 this interval decreases and additional narrow velocity intervals emerge. The latter are due to ballistic islands in the PSS of the RB. We remark that opposite to the frequency dependence (Fig. 9 a)), the corresponding velocity peaks are barely affected by changes of the amplitude. At least qualitatively, this behaviour can be understood by considering trajectories of particles within these ballistic islands: On the one hand the constant mean velocity of an island can be understood by remembering that ballistic islands correspond to synchronised orbits, where the particle collides with

the barrier at distinguished phases. Hence, their mean velocity only depends on the frequency rather than on the amplitude of the oscillation. On the other hand the precise point of appearance as well as the shape of the islands can very well depend on A_1 and has to be determined by numerical simulations.

The amplitude dependence of the transmission probability p_T is shown in Fig. 11 b), where -as before- we consider only particles that reach x_{mid} at least once. Evidently, p_T remains approximately unity for $0 \lesssim A_1 \lesssim 0.4$ and thereafter decreases steadily with further increasing A_1 , besides a weakly pronounced local maximum at $A \approx 0.8$. Following the arguments presented in the previous section, this behaviour is a result of the overlap of the chaotic sea in the LB and regular structures within the RB.

No relevant new phenomena are observed for the particles exiting at x_{\min} which is why we refrain from providing a discussion of this case.

C. Phase variations

Let us finally explore the impact of phase changes $\Delta\Phi_1$ for fixed $\omega_1 = 1.0$ and $A_1 \approx 0.57$. The phase velocity distributions at x_{\max} are shown in Fig. 8 i)-l). Fig. 8 i) and j) correspond to comparably small phase differences of $\Delta\Phi_1 = 0.1\pi$ and $\Delta\Phi_1 = 0.2\pi$ respectively. A comparison of these graphs with the one for $\Delta\Phi_1 = 0$ (Fig. 5 a)) reveals that the main difference is a small shift of the entire phase space to the region of smaller phase values. Consequently, the $n = 4$ island ($v \approx 3.2$) in the RB is not completely covered by the corresponding island in the LB anymore. Hence, the outer most curves can be populated by particles. The tendency that islands are moved to smaller values of the phases for increasing $\Delta\Phi_1$ is still apparent for $\Delta\Phi_1 = 0.5\pi$ as seen in Fig. 8 k). Additionally, the $n = 4$ island is fully populated by particles and more diffusive particles manage to reach x_{\max} . Finally, there are no particles in spanning curves above the FISC anymore. In contrast to the frequency and amplitude dependence, $\Delta\Phi_1$ has a substantial influence on the symmetries of the Hamiltonian and thus on the transport (cf. Fig.3). In fact for $\Delta\Phi_1 = 0.5\pi$ time reversal symmetry is restored ($d_1(t, \Delta\Phi_1 = 0.5\pi) = d_1(-t, \Delta\Phi_1 = 0.5\pi)$) and the directed current vanishes. Obviously, this increases the probability for a particle to traverse diffusively the RB, which explains the notable amount of non ballistic particles in Fig. 8 k). Finally, the transport in the RB is reversed, i.e. points in a positive direction, for $\Delta\Phi_1 = \pi$. Moreover we notice that $d_1(t, \Delta\Phi = \pi) = -d_1(t + \pi, \Delta\Phi = 0)$, i.e. the driving law in the RB equals the driving law in the left one besides an initial phase shift of π . Consequently, the ballistic islands for $d_1(t)$ are at the same velocities but at phases shifted by π . Since the PSS for $d_0(t)$ is 'almost' invariant under a shift of π , the overlap from the chaotic sea in the LB and regular structures in the right one is comparably

small for $\Delta\Phi_1 = \pi$. Thus, very few particles reach x_{\max} ballistically and the phase velocity distribution is dominated by chaotic particles (Fig. 8 l)).

Fig. 9 c) shows the $\Delta\Phi_1$ dependence of the phase integrated velocity distributions. We observe an increasing amount of diffusive particles for $\Delta\Phi_1$ close to $\Delta\Phi_1 = \pi$ compared to $\Delta\Phi_1 = 0$ (or $\Delta\Phi_1 = 2\pi$). As stated before, this is a consequence of the dependence of the direction of the current in the RB which is positively directed for $\Delta\Phi_1 = \pi$ while it is negatively directed for $\Delta\Phi_1 = 0$.

As a last remark on the two block setup the transmission probability p_T as a function of $\Delta\Phi_1$ is shown in Fig. 11 c) and reveals an oscillatory behaviour with local maxima at $\Delta\Phi_1 = 0, \pi$ and 2π . For frequency and amplitude variations we argued that the value of p_T is determined by the overlap of regular structures in the RB with the chaotic sea of the LB. However, in the present case, this overlap is minimal for $\Delta\Phi_1 = \pi$. Apparently, this decreasing overlap for $\Delta\Phi_1 \rightarrow \pi$ is compensated by an increasing probability for a particle to surpass the RB diffusively due to the positively directed current (cf. Fig.3).

VI. VELOCITY DISTRIBUTIONS IN SUPERLATTICES

In the previous sections we have demonstrated how a setup build up out of two blocks with different driving laws allows for conversion processes from diffusive-to ballistic motion. Even more we were able to control the velocity distributions for outgoing particles at x_{\max} by adjusting parameters in the RB. In the following we argue how the so far gained insights can be exploited to maintain mono energetic- pulsed particle beams out of diffusive particle ensembles in superlattices containing a few hundred blocks. The general outline of the used scheme is as follows: We start with an initially diffusive particle ensemble in the $B = 0$ block (with B being the block index, cf. Fig 1) which is transported towards a first interface where particles can be injected into ballistic islands of the $B = 1$ blocks phase space. The parameters in the driving laws are chosen such that these now ballistic particles travel opposite to the directed currents and thus we obtain a peaked velocity distribution at the end of the $B = 1$ block. For the following blocks with $B = 2, \dots, 100$ we show how the width of each peak in the velocity distribution can be tuned by adjusting the amplitude of the barrier oscillation blockwisely. As a last step, we demonstrate how an appropriate choice in the driving laws for $B > 100$ allows to preserve one of the peaks in the velocity distributions while the other peaks are subsequently removed. Thus we obtain a mono energetic particle beam for outgoing particles in the superlattice. Moreover, the beam is pulsed in a sense that the particles leave the systems only at distinguished phases.

A. Interface dynamics of ballistic particles

Before we start a detailed discussion of the physics in the BL containing a few hundred blocks, let us again consider the simple case of a two block setup to introduce a new type of conversion processes which occurs in larger BL namely ballistic to ballistic- or ballistic to diffusive conversion. To make our discussion more concrete we consider again a setup with driving laws as in section IV. Hence the PSS for the LB is shown in Fig. 2 c) and the PSS for the RB is shown in Fig. 2 d). In contrast to the previous discussions we explore the possible conversion processes for a ballistic particle arriving at the interface. For example, consider a particle beam started at x_{\min} which uniformly occupies the ballistic island at $(v = 1.8, \phi = 3\pi/2)$ (in Fig. 2 c)) and passes ballistically the LB. Apparently, these particles would be entirely injected into the chaotic sea of the PSS in the RB once they pass x_{mid} . Due to the negatively directed transport in the RB the particles are transported back to x_{mid} where they can again be injected into any regular structures of the PSS corresponding to the LB, or after several passings of x_{mid} into regular structures of the RB. Hence, the outgoing particles at x_{\max} for this initially mono energetic beam would occupy all accessible regular structures of the PSS of the RB and the corresponding velocity distribution at x_{\max} would contain multiple peaks.

As a second example we consider a particle beam (again started at x_{\min}) which passes the LB by uniformly occupying the ballistic island at $(v = 3.2, \phi = 3\pi/2)$. In this case, some particles are injected into the ballistic island in the RBs PSS at similar coordinates, while others become diffusive. The particles which remain ballistic traverse the RB and cause a dominant peak in the velocity distribution at x_{\max} . For the particles which become diffusive the same arguments hold as before. Thus these particles lead to less pronounced peaks in the velocity distribution at velocities corresponding to any kind of regular structure in the RB. Accordingly the initial particle beam was converted into a particle beam with a smaller width, because the ballistic island in the LB, i.e. for the initial beam, is larger than the island in the RB in which these particles are injected. In addition to this, peaks in the velocity distribution emerge due to injection of diffusive particles after multiple crossings of x_{mid} .

B. Amplitude variations in superlattices

In the following section we demonstrate how the previously discussed interface dynamics of ballistic particles can be exploited to narrow the velocity distribution of particles in an appropriately designed superlattice. To this end we consider a setup build up out of $N_{\text{Bl}} = 101$ blocks (whereas each block contains $N = 10^4$ barriers) which expands from $x_{\min} = 0$ to $x_{\max} = NLN_{\text{Bl}}$. Accordingly, the positions of the interfaces, i.e. the positions where the driving laws change, are given by

$x_B = NLB$ with $B = 1, \dots, 100$. For the $B = 0$ block the driving law is $d_0(t)$ with parameters as in Fig. 2 c) inducing a positively directed current. For $B = 1, \dots, 100$ the driving laws are: $d_B(t) = A_B[\cos(2.2t) + \sin(4.4t)]$ with $A_B = 0.3 + 0.07 \cdot B$ (i.e. the amplitude is slowly increased from 0.3 to 1.0) inducing negatively directed currents. The initial conditions for the simulated ensemble are $t = 0$, $0.4NL < x < 0.6NL$ and $-0.1 < v < 0.1$. Hence the particles are located within the chaotic sea of

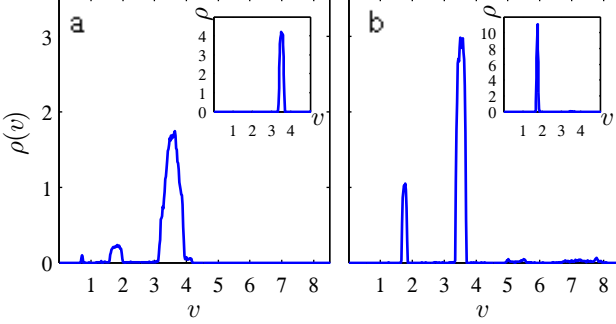


FIG. 12. Velocity distributions at positions a) $x_2 = 2NL$ and b) $x_{\max} = 101NL$. Parameters in $d_0(t)$ as in Fig. 4. For $0 < B \leq 100$ we set $d_B(t) = A_B[\cos(\omega_B t + \varphi_B) + \sin(2(\omega_B t + \varphi_B))]$ with $\omega_B = 2.2$, $\varphi_B = 0$ and $A_B = 0.3 + 0.07(B - 1)$. The inset in a) shows $\rho(v)$ at $x = 200NL$ with $\omega_B = 2.2$, $A_B = A_{101}$ and $\varphi_B = \pi(B - 1)$ for $100 < B \leq 200$. The inset in b) shows $\rho(v)$ at $x = 500NL$ with $\omega_B = 2.2$, $A_B = A_{101}$ and $\varphi_B = 0.02\pi(B - 1)$ for $100 < B \leq 500$.

the $B = 0$ block with driving law $d_0(t)$ and transported towards the first interface at $x_1 = NL$. At this point they can be injected into ballistic islands into the phase space in the $B = 1$ block. Since the local current in this block is negatively directed, it is hard to surpass for diffusive particles and we obtain a peaked velocity distribution at

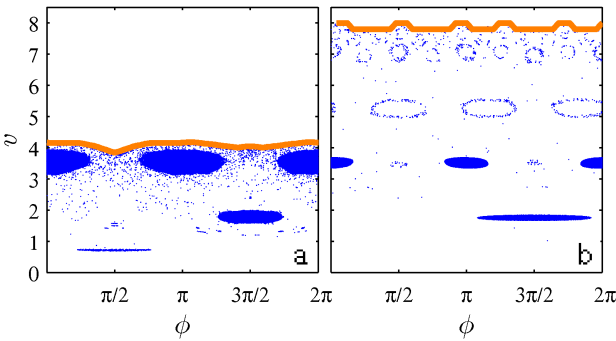


FIG. 13. Phase velocity distributions at a) $x = 2NL$ and b) $x = 101NL$. Orange line indicates the FISC. (Parameters as in Fig. 12).

$x_2 = 2NL$ (Fig. 12 a)) which is dominated by a peak at $v \approx 3.5$ and a less pronounced one at $v \approx 1.8$. The phase velocity distribution at $x_2 = 2NL$ (Fig. 13 a)) reveals that the dominant peak ($v \approx 3.5$) can be related to an island with winding number $n = 2$, while the second

peak ($v \approx 1.8$) is associated to a $n = 1$ island.

In the following blocks the amplitude of the barrier oscillation is subsequently increased and as a result we obtain a velocity distribution with two narrow peaks at the same velocities as before for particles at $x_{\max} = 101NL$ (Fig. 12 b)). Additionally, we observe some particles with velocities $v > 4.5$. The reason for the two dominant peaks is that the amplitude has (as argued in section V) only little influence on the position of ballistic islands in phase space. Thus, most particles remain ballistic at each interface. However the amplitude does have a notable influence on the size of the islands and by choosing the amplitude appropriately, one can tune the width of the velocity distribution by adjusting the size of the corresponding ballistic islands. In the present setup we exploit that an increasing amplitude leads to a decreasing size of the islands for the used parameters. Hence, the velocity distribution is squeezed when the particles propagate further into the superlattice. The fast particles with $v > 4.5$ correspond to particles in ballistic islands of the underlying phase space which is best seen in the phase velocity distribution at $x = 101NL$ (Fig. 13 b)). In fact, these are the in the previous section discussed peaks in the velocity distribution that emerge due to injection of diffusive particles after multiple crossings of an interface.

C. Peaked velocity distributions in superlattices

The last step to a mono energetic particle beam is to remove one of the peaks in Fig. 12 b) without losing too many particles in the other one. This can be done by exploiting the symmetries of both islands, which is achieved by adding more blocks to the superlattice with driving laws: $d_B(t) = 1.0[\cos(2.2t + \varphi_B) + \sin(4.4t + 2.2\varphi_B)]$ for $101 < B < 201$ with $\varphi_B = \pi(B - 1)$. Before we show the resulting velocity distributions, let us briefly discuss the idea behind the chosen driving laws: On the one hand we have seen that the peak at $v \approx 3.5$ corresponds to a $n = 2$ island and consists of two island structures at the same velocity but at different phases (cf. Fig. 13). Hence, an additional phase shift $\varphi = \pi$ in the driving law 'maps' both island into each other and most particles remain ballistic. On the other hand the $n = 1$ island which is responsible for the peak at $v \approx 1.8$ is 'mapped' into the chaotic sea for such a phase shift and particles in it become diffusive. Even though some of these now diffusive particles might be reinjected into a ballistic island of the following block, the majority is transported away. Consequently, after performing this procedure multiple times, one obtains a mono energetic particle beam. The resulting velocity distribution is shown in the inset of Fig. 12 a) and reveals that we obtain indeed the desired form of a mono energetic particle beam.

At this point we remark that the described technique of removing peaks according to the symmetry of their associated ballistic island works for a wide range of dif-

ferent parameter values as well as for ballistic islands with higher winding numbers. Unfortunately, it does not apply for the $n = 1$ island and thus we can not use it to remove the peak at $v \approx 3.5$ while keeping the one at $v \approx 1.8$. However, we can exploit that for a large amplitude the $n = 1$ island tends to cover a larger range of phases in the PSS (cf. Figs. 8 g) and h)). Hence, a small phase shift in the driving law removes relatively fewer particles in the $n = 1$ island compared to the ones with higher n . Following this idea, we choose $d_B(t) = A_{101}[\cos(2.2t + \varphi_B) + \sin(4.4t + 2.2\varphi_B)]$ for $101 < B < 501$ with $\varphi_B = 0.02\pi(B - 100)$ and the resulting velocity distribution at $x = 500NL$ is shown in the inset of Fig. 12 b). Again, we obtain the desired distribution of a monoenergetic particle beam.

VII. CONCLUSION

We have explored the classical non-equilibrium dynamics of particles in a one-dimensional driven superlattice which consists of blocks each containing many individual barriers. While similar systems that are usually studied in this context consist of lattices where all barriers are governed by the same time-dependent force, i.e. driving law, we allowed for a different driving in each block. In doing so we show that the thus obtained variability leads to remarkable new dynamical phenomena. To this end we analysed in detail how the blockwise variation of the driving law gives rise to conversion processes from diffusive- to ballistic motion and vice versa at the interfaces, i.e. the positions in the superlattice where the driving law changes. The combination of directed transport and these conversion processes enabled us to obtain

peaked velocity distributions in a simple system containing only two blocks with different driving laws providing oppositely directed currents. Additionally, we observed strong correlations between the phases and velocities for the escaping particles even though the initial particle ensemble is of exclusively diffusive character. Even more, we found that the velocity distributions as well as the correlations can be modified in a controlled manner by adjusting parameters such as frequency or amplitude in the driving. Finally, we present a scheme for superlattices containing a few hundred blocks by which a diffusive particle ensemble can be converted into a pulsed particle beam, whose mean energy and width in momentum space can be adjusted. Since this scheme mostly depends on simple symmetry arguments it is viable over a wide range of parameters. Thus it should be applicable to experimental setups, such as layered semiconductor heterostructures with different AC drivings or even to cold atom experiments in which counter propagating laser beams can create a one-dimensional lattice potential. By passing the laser beams through two acousto-optical modulators the desired AC drivings can be obtained.

As a future perspective it would be intriguing to explore -both theoretically as well as experimentally- the analogues of the presented effects in the quantum regime.

ACKNOWLEDGMENTS

C.P. thanks the Excellence Cluster Frontiers in Quantum Photon science, which is supported by the Joachim Herz Stiftung, for financial funding. We thank F.K. Diakonov for helpful discussions.

-
- [1] S. Wiggins, *Chaotic Transport in Dynamical Systems*, (Springer, Berlin, 1992).
 - [2] J. Maddox, *Nature* **365**, 203 (1993).
 - [3] R. Bartussek, P. Hänggi and J. G. Kissner, *Europhys. Lett.* **28**, 459 (1994).
 - [4] M. I. Dykman, H. Rabitz, V. N. Smelyanskiy and B. E. Vugmeister, *Phys. Rev. Lett.* **79**, 1178 (1997).
 - [5] M. O. Magnasco, *Phys. Rev. Lett.* **71**, 1477 (1993).
 - [6] F. Jülicher, A. Ajdari and J. Prost, *Rev. Mod. Phys.* **69**, 1269 (1997).
 - [7] A. V. Ponomarev, S. Denisov and P. Hänggi, *Phys. Rev. Lett.* **102**, 230601 (2009).
 - [8] S. Flach, O. Yevtushenko, and Y. Zolotaryuk, *Phys. Rev. Lett.* **84**, 2358 (2000).
 - [9] T. Dittrich, R. Ketzmerick, M.-F. Otto and H. Schanz, *Ann. d. Phys.* **9**, 755 (2000).
 - [10] S. Denisov and S. Flach, *Phys. Rev. E.* **64**, 056236 (2001).
 - [11] O. Yevtushenko, S. Flach, Y. Zolotaryuk and A. A. Ovchinnikov, *Europhys. Lett.* **54**, 141 (2001).
 - [12] S. Denisov, S. Flach, A. A. Ovchinnikov, O. Yevtushenko and Y. Zolotaryuk, *Phys. Rev. E.* **66**, 041104 (2002).
 - [13] S. Denisov, S. Flach and P. Hänggi, *Europhys. Lett.* **4**, 588-594 (2006).
 - [14] J. Gong and P. Brumer, *Phys. Rev. Lett.* **97**, 240602 (2006).
 - [15] L. Wang, G. Benenti, G. Casati and B. Li *Phys. Rev. Lett.* **99**, 244101 (2007).
 - [16] Special issue on Ratchets and Brownian Motors: Basics, Experiments and Applications, edited by H. Linke, *Appl. Phys. A* **75**, 167 (2002).
 - [17] H. Linke, T. E. Humphrey, A. Löfgren, A. O. Sushkov, R. Newbury, R. P. Taylor and P. Omling, *Science* **286**, 2314 (1999).
 - [18] K. N. Alekseev, M. V. Erementchouk and F. V. Kusmartsev, *Europhys. Lett.* **47**, 595 (1999).
 - [19] R. Gommers, S. Bergamini and F. Renzoni, *Phys. Rev. Lett.* **95**, 073003 (2005).
 - [20] R. Gommers, S. Denisov and F. Renzoni, *Phys. Rev. Lett.* **96**, 240604 (2006).
 - [21] T. Salger, S. Kling, T. Hecking, C. Geckeler, L. Morales-Molina and M. Weitz, *Science* **326**, 1241 (2009).
 - [22] A. Wickenbrock, P.C. Holz, N.A. Wahab, P. Phoonthong, D. Cubero and F. Renzoni, *Phys. Rev. Lett.* **108**, 020603

- (2012).
- [23] C. Petri, F. Lenz, F. K. Diakonov and P. Schmelcher, Phys. Rev. E. **81**, 046219 (2010).
- [24] B. Liebchen, C. Petri, F. Lenz and P. Schmelcher, Europhys. Lett. **94**, 40001 (2011).
- [25] C. Petri, F. Lenz, B. Liebchen, F. K. Diakonov and P. Schmelcher, Europhys. Lett. **95**, 30005 (2011).
- [26] P. Olbrich, J. Karch, E. L. Ivchenko, J. Kamann, B. März, M. Fehrenbacher, D. Weiss and S. D. Ganichev, Phys. Rev. B. **83**, 165320 (2011).
- [27] E. L. Ivchenko and S. D. Ganichev, JETP Letters, **93**, 673 (2011).
- [28] A. J. Lichtenberg and M. A. Leiberman, *Regular and Chaotic Dynamics*, (Springer-Verlag, Heidelberg, 1992, second edition).
- [29] N. R. Quintero, José A. Cuesta and Renato Alvarez-Nodarse, Phys. Rev. E. **81**, 030102 (2010).